DIrect Sunlight into CO conversion

De Vrijer, Thierry; Smets, Arno

DOI
10.1109/PVSC48317.2022.9938900

Publication date
2022

Document Version
Final published version

Published in
2022 IEEE 49th Photovoltaics Specialists Conference, PVSC 2022

DIrect Sunlight into CO conversion

Thierry de Vrijer, Arno Smets

Delft University of Technology, 2628 CD Delft, Netherlands

***Abstract*—in this abstract an overview is presented of research performed in the DISCO project, on the development of a silicon-based high voltage multijunction device for autonomous solar to fuel applications. "**

Keywords— solar-to-fuel, multijunction PV, silicon, germanium, high voltage

I. Introduction

In this abstract, the highlights of the DISCO project are discussed. In the DISCO project the processing of wireless silicon-based high-voltage 2-terminal multijunction (MJ) photovoltaic (PV) devices, is investigated. Such devices can be used in autonomous solar-to-fuel synthesis systems, as well as other innovative approaches in which the MJ solar cell is used not only as a photovoltaic current-voltage generator, but also as an ion-exchange membrane, electrochemical catalysts and/or optical transmittance filter. A prerequisite for the development of stand-alone solar-to-fuel synthesis devices is a wireless PV component that generates sufficient voltage to drive the desired electrochemical reduction reaction. The aim of DISCO is therefore to provide a framework that can be used for the flexible application of earth abundant and chemically inert Group IV alloys to realize a range of V_{oc}'s, facilitating electrochemical (EC) reactions ranging from water splitting to CO_2 reduction, in different wireless MJ architectures.

The framework is developed through the investigation of I. PV materials and single junction solar cells, including a plasma enhanced chemical vapour deposition (PECVD) processed group IV low bandgap alloy based on Ge(Sn):H, and II textures on c-Si. In these first two areas, research was focused on developing a better understanding of the fundamental relations between: i) processing parameters ↔ ii) material structure ↔ iii) opto-electrical properties & chemical stability ↔ iv) PV device performance. Here i) includes parameters like the deposition technique, substrate type/morphology, and conditions such as temperature, power pressure and ii) includes characteristics like the elemental composition/stoichiometry, void fraction, crystalline phase fraction.

Finally, in part III of DISCO, the additional challenges introduced in MJ architectures are considered. These include the structural investigation of the tunnel recombination junction (TRJ) as well as the J_{SC} vs V_{OC}*FF trade-offs as a function of absorber characteristics, such as elemental composition and thickness, and those introduced by using an intermediate reflective layer. Additionally, in DISCO, the design considerations for developing a Photoelectrochemical (PEC) device from a PV device are investigated.

II. DISCO results

A. Photovoltaic materials

The influence of individual deposition conditions is characterized in DISCO for a range of materials. These include hydrogenated (:H) doped Si and siliconoxide (SiO_X) [1], [2] as well as intrinsic SiGe:H [3], Ge:H [4]–[6] and GeCSn:H [7]. These detailed works do not only provide tools for achieving certain structural properties in the different materials, but also high-level relations between structural properties and the chemical stability and opto-electrical nature of the materials.

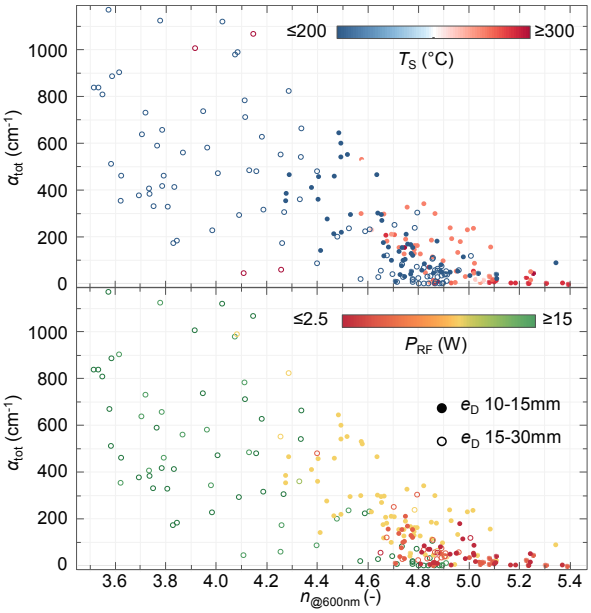

Fig.1: α_{tot} (metric for chemical instability) as a function of $n_{@600nm}$ for all Ge:H films processed in the DISCO project. Closed icons and open icons indicate samples processed with e_D≤15mm and e_D>15mm, respectively. Colour indicates T_S (top) and P_{RF} (bottom). From [8].

An example of the ii) material structure ↔ iii) chemical stability relation is shown in Fig.1, where the α_{tot}, a film-thickness independent metric for chemical stability [8] based on infrared oxidation and carbisation signatures [9], is plotted as a function of the refractive index at a wavelength of 600nm ($n_{@600nm}$), which can be considered a metric for the material density.

Fig.1 not only shows that the densest films do not suffer from post-deposition oxidation (α_{tot}=0) and that the degree of oxidation increases (α_{tot} ↑) with decreasing $n_{@600nm}$, it also demonstrated that the densest films are only realized in a specific processing window. This window involves relatively high

2022 IEEE 49th Photovoltaics Specialists Conference (PVSC) | 978-1-7281-6117-4/22/$31.00 ©2022 IEEE | DOI: 10.1109/PVSC48317.2022.9938900

substrate temperature (T_S), low RF power (P_{RF}) and a small electrode distance (e_D).

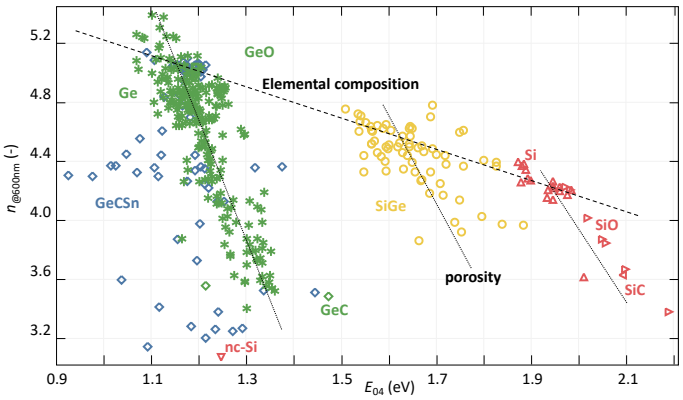

Fig. 2: $n_{@600nm}$ as a function of the E_{04} optical bandgap energy of a range of hydrogenated group IV alloys processed in the DISCO project. Trendlines indicating the effect of elemental compostion and porosity are referenced in text. From [8].

An example of the ii) material structure ↔ iii) opto-electrical properties relation is shown in Fig.2, where the optical bandgap energy (E_{04}) is plotted as a function of $n_{@600nm}$ for of over 400 films consisting of a wide range of group IV alloys. The influence of structural properties such as the elemental composition and porosity/void fraction, are indicated by the dashed lines.

Naturally, a lack of chemical stability on a film level is not desirable, as this will result either in potential trade-offs between performance and stability, or more complex and expensive encapsulation on a device level. The former trade-off is shown in Fig.3, which demonstrates that increasing the deposition pressure of the p- or n-doped SiO_X:H layer results in improved chemical stability of single junction p-i-n a-Si:H solar cells. However, this improvement comes at the cost of initial conversion efficiency, as the opto-electrical qualities of the doped SiO_X:H films are reduced when the chemical stability is improved.

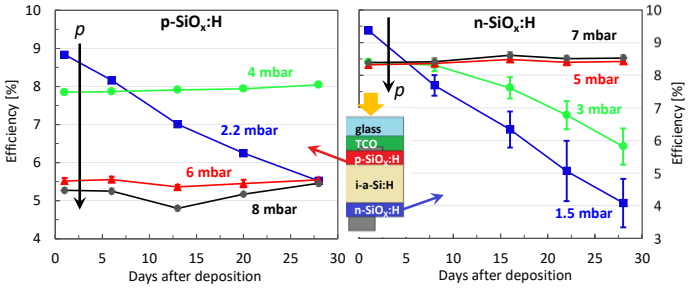

Fig. 3: Evolution over time of the conversion efficiency of single junction a-Si:H p-i-n superstrate PV devices. Coloured curves indicate depostion pressure of the p-SiO_X:H layer (left) and n-SiO_X:H layer (right). From [1].

B. Textures on c-Si

Surface textures that result in high optical yields are crucial for high efficiency PV devices. Some of the architectures investigated in DISCO combine a crystalline (c-) silicon heterojunction with a thin film silicon junction with a nanocrystalline (nc-) absorber. This nano-crystalline material is incompatible with the relatively steep slopes of the conventional <111> crystal orientation. For that reason, several texturing approaches were explored for developing smooth concave surface features on mono-c-Si. Four approaches were explored, resulting in widely different surface morphologies, as shown in Fig.4. The figure demonstrates that three of the 4 textures could sustain the growth of crack-free device-quality nc-Si:H. For the periodic honeycomb texture (right) this requires some tuning of periodicity and radius.

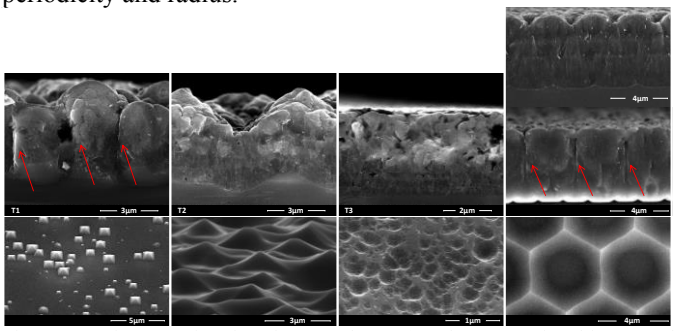

Fig. 4: SEM images of surface features (bottom) and cross sectional images of a 3-5um nc-Si:H layer grown on top of the textured silicon (top) of the different textures on mono-c-Si developed in the DISCO project. Red arrows indicate cracks fromed in the nc-Si:H layer in the focal point of steep features. From [10] and [11].

The influence of the various processing steps in each of the different approaches was extensively characterized. This characterization revealed the relation between the surface morphology and optical behavior, both in terms of overall light in-coupling and light-scattering, as well as the tunability of spectrally dependent scattering of the periodic surface features. Additionally, the performance of devices grown on the different textures was compared both through optical simulations, as demonstrated in Fig.5, as well as experimentally. The latter revealed the trade-offs between surface roughness related optical gains and V_{oc}*FF losses.

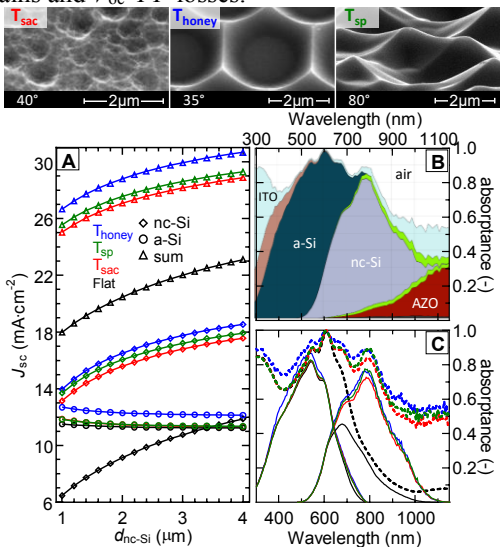

Fig. 5: Simulated performance of a-Si/nc-Si tandem devices on flat substrates and substrates with T_{sac} (red), T_{sp} (green) and T_{honey} (blue) textures (textures indicated by SEM images). **A** shows the J_{SC} of the a-Si junction, nc-Si junction and the sum of both junctions, for different textures, as a function of nc-Si absorber thickness (d_{nc-Si}). **B** shows the spectral absorptance in each of the layer of the tandem device on T_{honey}. **C** shows the a-Si and nc-Si absorptance curves

and 1-*R* curves for the different substrate types, for tandem device with $d_{a\text{-}Si}$=300nm and $d_{nc\text{-}Si}$=1.2µm. From [11].

C. *Multijunction devices*

Having developed a better understanding of the materials on a film and single junction device level, part III of DISCO focused on MJ devices. In [12], the qualitative fundamental working principles of TRJ's based on p- and n-doped Si(O_X) alloys are revealed using both electrical modelling and experiments based on a unique set of tandem lab cells (four types based on four different PV materials) combined with structural variations in TRJs architectures. The study resulted in design rules for the integration of silicon-oxide based TRJs and provides fundamental insights into the sensitivity of the electrical performance of the TRJ's to doping concentrations, to alignment of the conduction and valence bands of consecutive sub-cells, to the nature of interface defects, to the growth of amorphous and crystalline phases and its dependence on substrate or seed layers and to the nanoscale thicknesses of the TRJ layers.

Then, in [13], optimal current matching in MJ devices is investigated. Specifically, the influence was studied of variations in absorber thickness as well as thickness variations of different intermediate reflective layers based on SiO_X, various transparent conductive oxides and metallic layers on all-silicon MJ PV devices. Using the design rules from this study, the SHJ/nc-Si:H(/a-Si:H) devices, shown in Fig.6, are processed with a V_{oc}≈2V and conversion efficiencies close 15%, the highest reported conversion efficiency for an all-silicon solar cell that generates at least 1V.

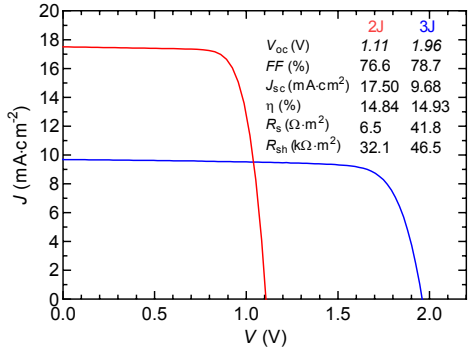

Fig. 6: The *J-V* and *EQE* curves of the champion 2J and 3J devices. An *EQE* diagram of the champion device, including all three subcells as well as the sum of three subcells and 1-*R* curves (dashed line) is presented. From [13]

In addition to the optimization of this particular device architecture, the flexible application of earth abundant and chemically inert silicon and silicon-germanium alloys is demonstrated in two distinct device architectures, as shown in Fig.7, combining up to 4 different junctions, yielding a relatively continuous V_{oc} range of 0.5V to 2.8V. The figure and the V_{oc}'s presented therein, can be used as a framework for selecting a suitable device architecture for facilitating a range of wireless and autonomous photo-electrochemical devices by fulfilling the voltage requirement for a range of electrochemical reduction reactions and electrocatalysts.

Finally, converting a multijunction PV device into a PEC device capable of continuous, autonomous stand-alone operation, requires the use of electrocatalytically active contacts and the development of micropores through the PV device to prevent large pH-gradient related overpotentials. Therefore, in DISCO, the influence of the size and distribution of micropores on the photovoltaic performance and electrochemical performance of a PEC device is simulated.

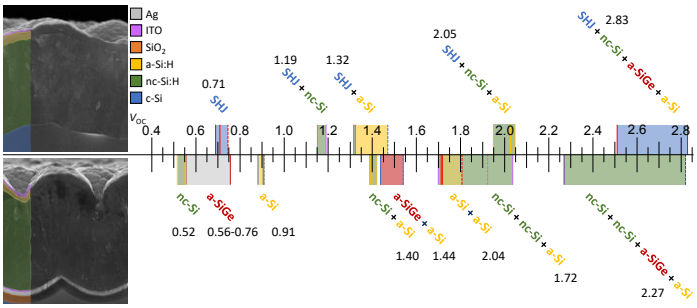

Fig. 7: V_{OC} range of different single- and multijuction PV device architectures. Top row indicates SHJ and hybrid SHJ and thin film silicon (SHJ+) multijunction devices. Bottom row indicates thin film silicon devices. Cross-sectional SEM images indicate the device architectures of the SHJ+ and thin film silicon multijunction devices. Colours added in the SEM images represent different materials, as indicated by the legend. In the V_{OC} range, 3 lines are present for each device architecture. Of these, the two solid lines indicate the highest measured V_{OC} and the V_{OC} of the device with the highest V_{OC}**FF* product processed in our lab. Highest measured V_{OC}'s are also indicated next to the device architectures. The dashed line indicates the V_{OC} of devices with the highest reported conversion efficiency, for which references can be found in [14].

It was shown that the influence on PV and EC performance is opposite in trend and that current density losses can be limited to less than 20% for a range of pore diameter-period combinations Additionally, as shown in Fig.8, the successful processing of micropores using deep reactive ion etching, and the processing of Pt microdots with a 2µm diameter and 5% surface coverage is demonstrated

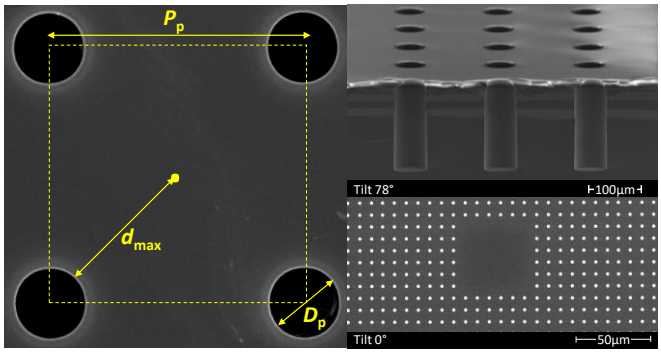

Fig. 8: SEM image of the surface of a porous substrate with D_p, P_p and d_{max} schematically indicated (left). Cross-sectional SEM image of pores with D_p=60µm processed partly through the wafer (right, top). SEM images of the substrate surface following successful Pt microdot application (right, bottom). From [14]

III. Conclusion

In this abstract an overview is presented of the DISCO project, where a framework is developed for the processing of high-voltage wireless silicon-based monolithically integrated 2-terminal multijunction photovoltaic devices. That can be used for stand-alone solar-to-fuel synthesis devices and other innovative PV applications.

ACKNOWLEDGMENT

The authors would like to gratefully acknowledge the financial support from the Netherlands Organization for Scientific Research (NWO) Solar to Products grant awarded to Arno Smets and the support provided by Shell International Exploration & Production Dense Energy Carriers Program.

REFERENCES

[1] T. de Vrijer, F. T. Si, H. Tan, and A. H. M. Smets, "Chemical Stability and Performance of Doped Silicon Oxide Layers for Use in Thin-Film Silicon Solar Cells," *IEEE J. Photovoltaics*, vol. 9, no. 1, pp. 3–11, 2019, doi: 10.1109/JPHOTOV.2018.2882650.

[2] T. de Vrijer and A. H. M. Smets, "The Relation Between Precursor Gas Flows, Thickness Dependent Material Phases, and Opto-Electrical Properties of Doped a/nc-$SiO_{X\geq0}$:H Films," *IEEE J. Photovoltaics*, vol. 11, no. 3, pp. 591–599, 2021, doi: 10.1109/JPHOTOV.2021.3059940.

[3] T. de Vrijer, H. Parasramka, S. J. Roerink, and A. H. M. Smets, "An expedient semi-empirical modelling approach for optimal bandgap profiling of stoichiometric absorbers: A case study of thin film amorphous silicon germanium for use in multijunction photovoltaic devices," *Sol. Energy Mater. Sol. Cells*, vol. 225, p. 111051, 2021, doi: 10.1016/j.solmat.2021.111051.

[4] T. de Vrijer, A. Ravichandran, B. Bouazzata, and A. H. M. Smets, "The impact of processing conditions and post-deposition oxidation on the opto-electrical properties of hydrogenated amorphous and nano-crystalline Germanium films," *J. Non. Cryst. Solids*, vol. 553, p. 120507, 2021, doi: 10.1016/j.jnoncrysol.2020.120507.

[5] T. de Vrijer, J. E. C. van Dingen, P. J. Roelandschap, K. Roodenburg, and A. H. M. Smets, "Improved PECVD processed hydrogenated germanium films through temperature induced densification," *Mater. Sci. Semicond. Process.*, vol. 138, p. 106285, 2022, doi: 10.1016/j.mssp.2021.106285.

[6] T. de Vrijer, B. Bouazzata, and A. H. M. Smets, "Spectroscopic review of hydrogenated , carbonated and oxygenated group IV alloys," *Vib. Spectrosc.*, under review.

[7] T. de Vrijer, K. Roodenburg, F. Saitta, T. Blackstone, G. Limodio, and A. H. M. Smets, "PECVD Processing of low bandgap-energy amorphous hydrogenated germanium-tin (a-GeSn:H) films for opto-electronic applications," *Appl. Mater. Today*, vol. 27, p. 101450, 2022, doi: 10.1016/j.apmt.2022.101450.

[8] T. de Vrijer *et al.*, "Opto-electrical properties of group IV alloys : the inherent challenges of processing hydrogenated germanium," *Adv. Sci.*, accepted for publication, 2022.

[9] T. de Vrijer and A. H. M. Smets, "Infrared analysis of catalytic CO2 reduction in hydrogenated germanium," *Phys. Chem. Chem. Phys.*, 2022, doi: 10.1039/D2CP01054B.

[10] T. de Vrijer and A. H. M. Smets, "Advanced textured monocrystalline silicon substrates with high optical scattering yields and low electrical recombination losses for supporting crack-free nano- to poly-crystalline film growth," *Energy Sci. Eng.*, vol. 9, no. 8, pp. 1080–1089, 2021, doi: 10.1002/ese3.873.

[11] T. de Vrijer *et al.*, "The optical behavior of random and periodic textured crystalline silicon surfaces for photovoltaic applications," *Prog. Photovoltaics Res. Appl.*, under review

[12] T. de Vrijer *et al.*, "The fundamental operation mechanisms of nc-$SiO_{X\geq0}$:H based tunnel recombination junctions revealed," *Sol. Energy Mater. Sol. Cells*, vol. 236, p. 111501, 2022, doi: 10.1016/j.solmat.2021.111501.

[13] T. de Vrijer, S. Miedema, T. Blackstone, D. van Nijen, C. Han, and A. H. M. Smets, "Application of metal, metal-oxide and silicon-oxide based intermediate reflective layers for current matching in autonomous high voltage multijunction photovoltaic devices," *Prog. Photovoltaics Res. Appl.*, under review

[14] T. de Vrijer, *High Voltage Photovoltaic Devices for Autonomous Solar-to-Fuel Applications*. Delft University of Technology, 2022.